LOCAL DEFORMATIONS CAUSED BY AN AIRCRAFT IMPACT ON A CONTAINMENT BUILDING

Jari Puttonen
Pentti Varpasuo

Rakenteiden Mekaniikka, Vol. 17
No 2 1984, s. 56...74

SUMMARY: This study was carried out to find a sufficient wall thickness for a containment building against an aircraft impact. The used load-time function simulates the impact of a military aircraft with the weight of 20 tons and velocity of 200 m/s. The outside radius of the dome was taken to be 24 m. Because of the essentially nonlinear nature of the problem both geometric and material nonlinearities were considered in the analysis. A suitable computer code to solve this kind of problems is PISCES-2DELK developed by Physics International Company. Description of the material behaviour was made using the Mohr-Coulomb model and taking into account the limits specified for allowable concrete deformations in Finnish code for reinforced concrete. This had to be made by inspection of the deformation histories because the model does not set a limit for concrete deformations in compression; however the concrete cracking is taken into account which is the essential condition for a reasonable analysis. The limit for concrete deformation in compression was set to 0.35 % and this failure criterium led to the wall thickness of over 2 meters, which was considerably more than obtained by previous analyses of similar nature. The effect of the amount of reinforcement was also investigated, and found to be nonessential. The main signifigance of the reinforcement was to secure the integrity of the concrete, and it can be neglected when the energy absorption characteristics of the structure are considered. The absorbed energy is mainly distorsion energy and the contribution of the concrete to this energy absorption is over fifteen times greater than that of the reinforcement. The area where structural deformations are considerable is small; outside a radius of 3 meters from the impact center the deformations are small. If the thickness of the containment building is 2.1 m then the maximum displacement is 0.35 m. In this case damages caused by the impact are easily reparable. However, complete safety against scabbing is reached only by using the steel liner.

INTRODUCTION

The analysis of a containment building behaviour in case of an aircraft impact may be divided into two different parts. In global analyses the overall response of a structure is considered. In this case linear theory of elasticity can usually be applied. The nonlinear effects of an aircraft impact are significant only locally and have a small effect on the overall behaviour of the structure /1/. In local analyses the effects that have to be taken into account are exactly these nonlinear phenomena which consist of the geometrical and material nonlinearities of the structure. So it is quite understandable that the ordinary methods of

structural analysis are ineffective and misleading in the simulation of structural behaviour in the vicinity of an impact area. This is the reason why several empirical formulae, as ACE-, NCRD-, BRL- and IRS-FORMULA /2/, have been developed to estimate the penetration depth, perforation- and scabbing thicknesses for a concrete target subjected to an impact load. These formulae have also been used to determine the effects of an aircraft impact in nuclear power plants. Because of the scale difference between the test models on which the empirical formulae were based and the containment buildings to which the aircraft impact was hypothetized, the results given by these formulae can not be entirely reliable, and may lead to erroneous results. A suitable computer code for analysing the local effects of an aircraft impact is PISCES-2DELK developed by the Physics International Company. This is a two-dimensional explicit finite difference scheme capable to solve dynamic structural and flow problems. Because of the two-dimensional geometry presentation of the program the apex of the containment dome was taken to be the impact location of the aircraft so that an axisymmetric model could be utilized.

The aim of this study is to give an estimation for the sufficient thickness of the containment wall capable to withstand an aircraft impact and secure the integrity of the containment so that it can be restored to its original condition with the aid of only minor reparations.

IMPACT LOAD

In the following the method for determining the shape of the time dependence of the impact force will be briefly exposed /3/. The geometry of the impacting object and the target at the beginning of impact (time $t = 0$) and during the impact (time $t > 0$) have been presented in Figure 1. The following assumptions are made in the analysis: 1) The analysis is essentially one-dimensional i.e. the deformations of the impacting object perpendicular to the x-axis are neglected and also the target is completely defined by its position coordinate along the x-axis ($X_A(t) = L + s(t)$ Figure 1); 2) The deformations of the missile are restricted to the area a from the impact point so that the x-coordinate of the beginning of the deformed area is $X_A(t) - a = L + s(t) - a$ (Figure 1); 3) The deformations of the target are presented by the time dependency of the location of the target ($s = s(t)$ Figure 1).

The governing equation of the motion for the missile will be derived as follows. From Figure 1 the expression for the velocity distribution is

$$u(x,t) = \dot{r}h(x-r) - (\dot{r} - \dot{s})h(x-(L+s-a)) - \dot{s}h(x-(L+s)) \qquad (1)$$

Where h( ) is the Heaviside step function and the time derivation is denoted by a dot.

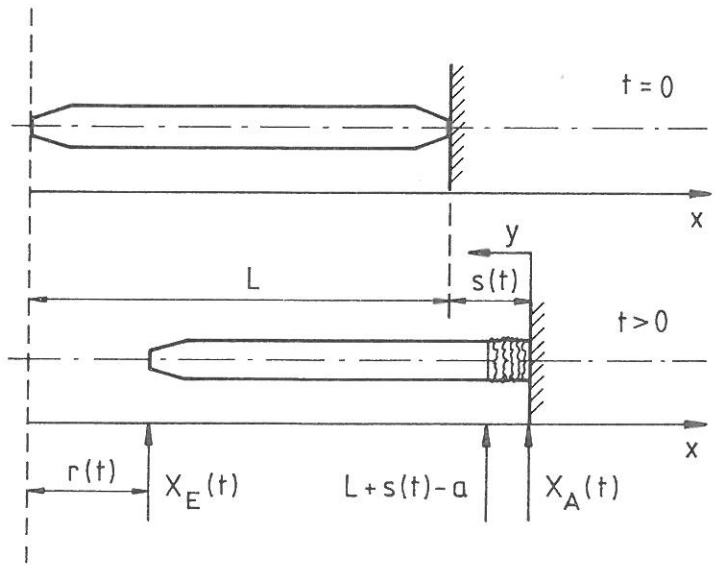

Figure 1. The geometry of the impacting object and the target.

If the total time derivative of u is denoted by $du(x,t)/dt$ and the mass for the unit length is denoted $m(x,t)$ then the equation of motion can be written in integral equation form as follows (Figure 1)

$$\int_{X_E(t)}^{X_A(t)} m(x,t)\,\frac{du(x,t)}{dt}\,dx - k(X_A(t)) + k(X_E(t)) = 0 . \qquad (2)$$

Here $k(X_A(t))$ and $k(X_E(t))$ are forces at the end points of the missile. Substituting expression (1) into equation (2) and taking into account that the rear end of missile is free we obtain an equation

$$\int_{r}^{L+s} m\,\frac{du}{dt}\,dx = \ddot{r}\int_{r}^{L+s-a} m\,dx + \ddot{s}\int_{L+s-a}^{L+s} m\,dx - (\dot{r}-\dot{s})^2 m(L+s-a) = k(X_A(t)) . \qquad (3)$$

In equation (3) the integral from L+s-a to L+s represents the mass of the aircraft

that is crashed on the contact surface during the time interval from zero to t. Using the mass distribution of the original undamaged aircraft $m_0(y)$ this mass can be written as follows

$$M_z(t) = \int_{y=0}^{r-s} m_0(p)\,dp \ , \tag{4}$$

where y is the coordinate from the head of the aircraft to the direction of the negative x. The mass of the undeformed part of the aircraft at time t is correspondingly

$$M_u(t) = \int_{y=r-s}^{L} m_0(p)\,dp \ , \quad M_0 = \int_0^L m_0(p)\,dp. \tag{5}$$

Substituting expressions (4) and (5) into equation (3) we obtain

$$\ddot{r}\, M_u(t) + \ddot{s} M_z(t) - (\dot{r}-\dot{s})^2 m_0(r-s) = k(X_A(t)). \tag{6}$$

At the interface between the undeformed and grossly deformed parts of the aircraft the crushing load F_B is acting at every moment of time. So the equation of motion for the undeformed portion of the aircraft can be written as follows

$$M_u(t)\ddot{r} = - F_B(r-s). \tag{7}$$

Finally the expression for the reaction force between the impacting aircraft and the target $k(t) = - k(X_A(t))$ is obtained from equations (6) and (7):

$$k(t) = + F_B(r-s) + (\dot{r}-\dot{s})^2\, m_0(r-s) - \ddot{s} M_z(t). \tag{8}$$

The nonlinear differential equation (7) is split into two first order equations as follows

$$\left.\begin{aligned} \dot{r} &= v \ , \\ \dot{v} &= - \frac{F_B(r-s)}{M_0 - \int_0^{r-s} m_0(p)\,dp} \ . \end{aligned}\right\} \tag{9}$$

The initial conditions for the equation system (9) are as follows

$$\left.\begin{aligned} r(0) &= 0,\ v(0) = v_0\ , \\ s(0) &= 0,\ \dot{s}(0) = 0. \end{aligned}\right\} \tag{10}$$

The equation system (9) together with initial conditions (10) is solved using finite difference approximations for the derivatives. If the function value at time point n is denoted by the right superscript then the finite difference equations corresponding to equations (9) and (8) can be written as follows

$$\left.\begin{aligned} v^{(n+1)} &= v^{(n)} - \Delta t\ \frac{F_B^{(n)}}{M_o - M_z^{(n)}}\ , \\ r^{(n+1)} &= r^{(n)} + \Delta t\ v^{(n+1)}\ , \\ k^{(n)} &= F_B^{(n)} + (v^{(n)} - \dot{s}^{(n)})^2 m_o (r^{(n)} - s^{(n)}) - M_z^{(n)} \ddot{s}^{(n)}. \end{aligned}\right\} \tag{11}$$

In order to use expressions (11) in numerical calculations in a specific example, the mass distribution m_0 and the distribution of the load carrying cross-section Q along the axis of the aircraft have to be specified. These distributions are presented in Figure 2.

The crushing load F_B along the longitudinal axis of the aircraft body is given by the equation

$$F_B = Q\,\sigma_{max}\ ,\quad \sigma_{max} = 5{\cdot}3{\cdot}10^8\ \frac{N}{m^2}\ . \tag{12}$$

In the following numerical example the wall is assumed to be infinitely rigid so that the motion s(t) of the target in equations (11) is set identically to zero. The total weight of the aircraft is taken to be 20 tons and the impact velocity 200 m/s. The time dependency of the impact force is given in Figure 3. The dashed line is the shape of the impact force calculated using equations (11). The time step was taken to be 0.00025 s and 0.00050 s. The difference in results using these two values for the time step was less than 0.5 MN. The solid line in Figure 3 corresponds to the load function used in the subsequent PISCES-calculations.

This load function corresponds to the IRS-formula for an aircraft of Phantom RF-4E type /4/ with slight modifications. The impact area is supposed to be a circle with the radius of 1.6 m so that the area is 8 m^2. The above derivation neglects the effects of the inertia and plastification of the target and the interaction between the target and the impacting object so that the load function thus derived is usually very conservative.

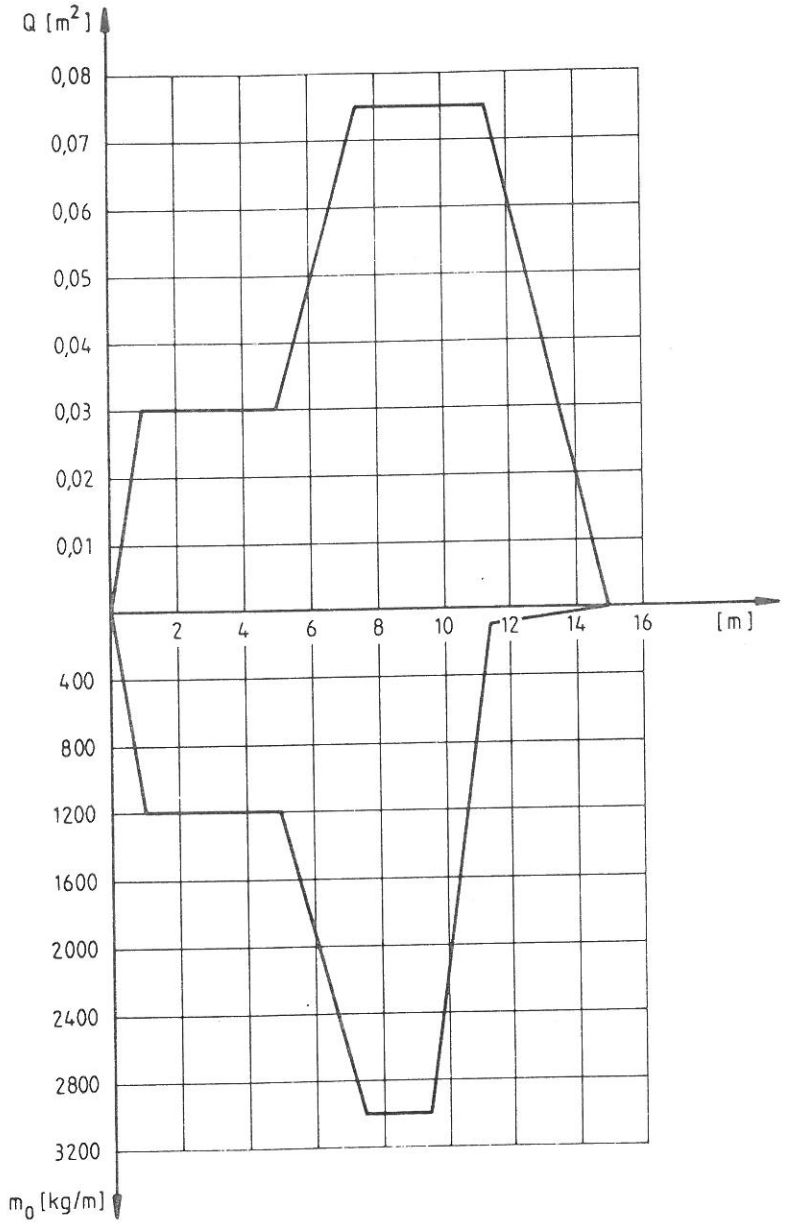

Figure 2. The cross-section and mass distribution along the longitudinal axis of the undeformed aircraft.

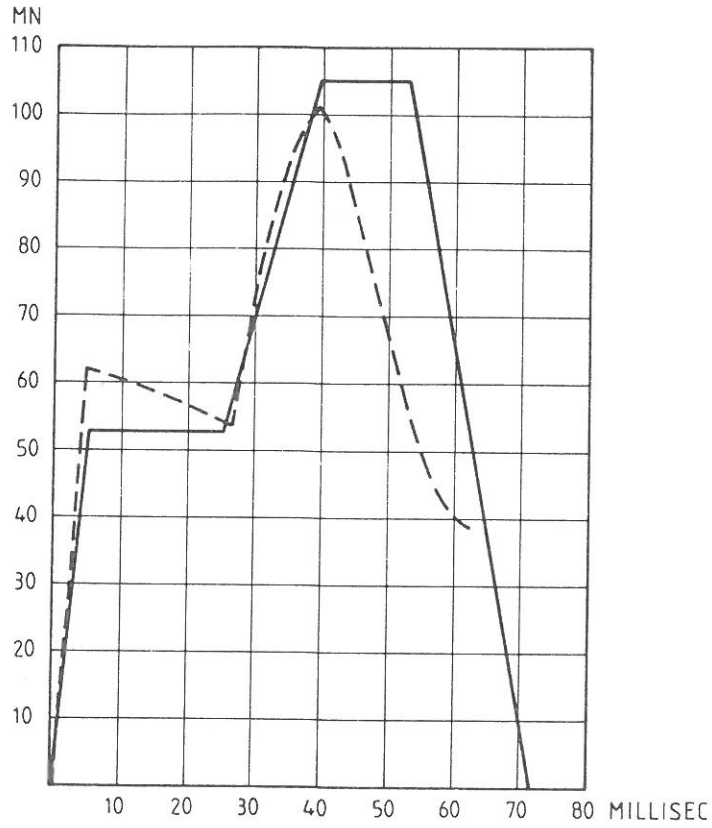

Figure 3. The calculated (dashed line) and standardized (solid line) load-time history of an aircraft impact.

MATERIAL MODELS

In the description of steel properties the von Mises yield model without work-hardening is adopted. The yield strength for the steel was taken to be 460 MN/m^2. In this value the increase of 15 % due to the dynamic load effect is taken into account. The values of the Young modulus and Poisson ratio were $2.1 \cdot 10^5$ MN/m^2 and 0.30, respectively. For steel density the value of 8000 kg/m^3 has been used.

The von Mises model is totally unsuitable for concrete. The design practice as it is presented in codes for reinforced concrete is somewhat ambiguous. Sometimes the tensile strength of concrete is neglected, for instance, in bending but taken into account in other cases as in shear. A realistic constitutive model for con-

crete and yet simple enough so that it can be defined with the aid of only few parameters seems to be the Drucker-Prager model /5/. It uses a criterion in which an envelope of Mohr-circles in the σ-τ plane describes the limit conditions. The envelope can be described by a linear variation of the radius of the Mohr-circles with the variation in the mean stress on the spherical part of the stress tensor. In three-dimensional state of stress the Drucker-Prager yield model is of the form:

$$f = \alpha I_1 + (J_2)^{1/2} - \bar{\sigma}/\sqrt{3} = 0 \tag{13}$$

in which

I_1 is the first invariant of the stress tensor, i.e.

$I_1 = \sigma_{ii} = \sigma_x + \sigma_y + \sigma_z = -3p$,

J_2 is the second invariant of deviatoric stress tensor, i.e.

$J_2 = \frac{1}{2} S_{ij} S_{ij} = 1/6[(\sigma_x-\sigma_y)^2-(\sigma_y-\sigma_z)^2-(\sigma_x-\sigma_z)^2]+\tau_{xy}^2+\tau_{xz}^2+\tau_{yz}^2$.

The constants α and $\bar{\sigma}$ can be related to the cohesion c and angle of friction φ of the material by the relations

$$\sin\varphi = \frac{3\alpha}{(1-3\alpha^2)^{1/2}} \quad , \quad c = \frac{\bar{\sigma}}{(3(1-12\alpha^2))^{1/2}} \quad . \tag{14}$$

In principal stress space the Drucker-Prager formulation of equation (13) represents a circular cone with its apex on the tension side. An associated flow rule for yield surface (13) gives the plastic strain rate

$$\dot{\epsilon}^P_{ij} = \lambda \partial f/\partial \sigma_{ij} = \lambda \left[\alpha\delta_{ij} + S_{ij}/2\, J_2^{\frac{1}{2}}\right] \tag{15}$$

where δ_{ij} is the Kronecker delta. Equation (15) shows that there will be a rate of plastic cubical dilatation

$$\dot{\epsilon}^P_{ii} = 3\alpha\lambda \ . \tag{16}$$

In the PISCES code the Drucker-Prager model is presented in the form

$$Y = ap + b \tag{17}$$

where

$Y = (3\, J_2)^{\frac{1}{2}}$ is equivalent for yield,

$p = -(\sigma_x+\sigma_y+\sigma_z)/3$ is the hydrostatic pressure.

a and b are material constants which can be related to the constants given in equations (14) by the expressions

$$a = 3\alpha\sqrt{3} \ , \quad b = \bar{\sigma} = c(3(1-12\alpha^2))^{\frac{1}{2}} \ . \tag{18}$$

The flow rule used in the PISCES code is non-associated to the yield model (13) and is equivalent to the flow rule of a von Mises material. This means that if the yield stress is exceeded, indicated by a stress state where Y is exceeded, the stress deviators are scaled down to bring them back on the yield surface. By the use of this non-associated flow rule there is no dilatancy due to yield.

The material parameters a and b in equation (17) are determined from the standard strength parameters of the concrete. The compression strength of the concrete is taken to be 30 MN/m^2 and the tensile strength 2.25 MN/m^2. Assuming that the tensile strength corresponds to the failure at uniaxial tension, the cohesion c can be calculated from the Mohr circle drawn at the tensile side. Taking the angle of friction φ of the concrete to be 30° and drawing the corresponding tangent to the Mohr circle, the cohesion is the line segment which the tangent extracts from the τ-axis. So we have for c the value 1.95 MN/m^2 and for constants a and b

$$\left.\begin{aligned} a &= 3\sqrt{3}\left(\frac{\sin^2\varphi}{3\sin^2\varphi+9}\right)^{\frac{1}{2}} = 0.836 \ , \\ b &= \bar{\sigma} = c\left(3\left(1-12\,\frac{\sin^2\varphi}{3\sin^2\varphi+9}\right)\right)^{\frac{1}{2}} = 2.81 \ MN/m^2 . \end{aligned}\right\} \tag{19}$$

Two additional parameters are specified for the Drucker-Prager model used in PISCES. These parameters are not included in the general yield model given by equation (13). They are the maximum yield strength from where on the material behaves as a von Mises material and the spall limit on the tensile side which cuts off the cone of equation (13) by certain value of the negative pressure p which means that when this failure pressure is reached the material is not allowed to transmit stresses any more. To represent the elastic domain of the concrete the values of $4.5 \cdot 10^4$ MN/m^2 and 0.20 are used for the Young's modulus and Poisson ratio, respectively. The graphical presentation of the used concrete model is shown in Figure 4.

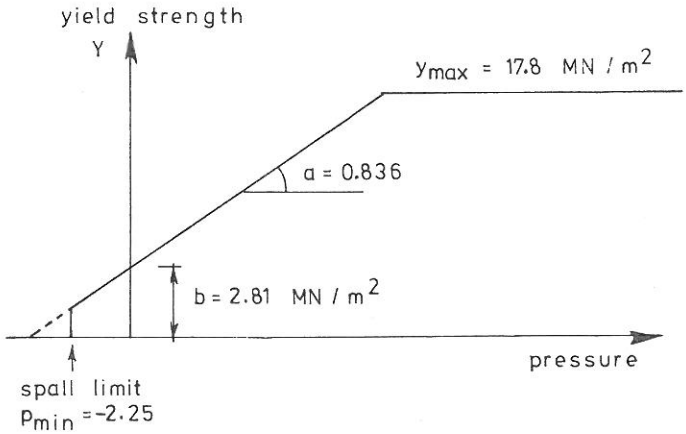

Figure 4. Material model of concrete (cubic compr. strength = 30 MN/m^2).

THE METHOD OF ANALYSIS AND THE USED FINITE DIFFERENCE MODEL

PISCES 2DELK is a two-dimensional, time-dependent finite difference code that can be applied to solve dynamic structural and flow problems as well as fluid-solid interaction problems. The organization of the code is based on so called processors which are attached to specific part of the finite difference grid and correspond to the formulation of different physical phenomena. At present state the code consists of four processors which are: 1) Lagrange-processor that is the formulation suitable for the problems of solid, continuous medium; 2) Shell-processor that is based on thin shell theory; 3) Euler-processor that is best suited for fluid flow problems and 4) Rigid-processor for describing the motion of infinitely rigid objects. The Lagrange-processor uses the Lagrange formulation of the continuum motion. The differential equations that govern the problem are applied to a network of zones that describes the geometry of the domain to be investigated. According to Langrangian formulation each zone contains a constant mass element of material that moves and distorts in space and time. The motion of all zones approximate the continuous motion. In a two-dimensional analysis two space variables exist and the third is determined from symmetry conditions. The partial differential equations that govern the motion in case of axial symmetry when x-axis is the symmetry axis are /6/ the momentum equations

$$\left.\begin{aligned} \rho\,\ddot{x} &= \frac{\partial \sigma_{xx}}{\partial x} + \frac{\partial \sigma_{xy}}{\partial x} + \frac{\sigma_{xy}}{y} \quad , \\ \rho\,\ddot{y} &= \frac{\partial \sigma_{yy}}{\partial y} + \frac{\partial \sigma_{xy}}{\partial x} + \frac{\sigma_{yy}-\sigma_{\theta\theta}}{y} \quad , \end{aligned}\right\} \tag{20}$$

the continuity equation

$$\frac{\dot{V}}{V} = \frac{\partial \dot{x}}{\partial x} + \frac{\partial \dot{y}}{\partial x} + \frac{\partial \dot{y}}{\partial y} \quad , \tag{21}$$

and the energy equation

$$\dot{E} = -(p+q)\dot{V} + V\left[S_{xx}\frac{\partial \dot{x}}{\partial x} + S_{yy}\frac{\partial \dot{y}}{\partial y} + S_{\theta\theta}\frac{\dot{y}}{y} + \sigma_{xy}\left(\frac{\partial \dot{y}}{\partial x} + \frac{\partial \dot{x}}{\partial y}\right)\right] + \dot{Q} \quad . \tag{22}$$

Here ρ is mass density,
$x, y, \dot{x}, \dot{y}, \ddot{x}, \ddot{y}$ are independent Lagrangian position, velocity and acceleration components,
$\sigma_{xx}, \sigma_{yy}, \sigma_{xy}, \sigma_{\theta\theta}$ are stress components,
S_{xx}, S_{yy}, $S_{\theta\theta}$ are stress deviator components,
p is hydrostatic pressure,
q is artificial von Neumann viscosity,
V is relative volume ρ/ρ_0, ρ_0 is reference density,
E is internal energy per original volume and
$\dot{Q}$ is heat flux.

Each zone in the finite difference network has a fixed mass. The calculations are divided in two types-grid point and zone. Associated with each grid point is the Lagrange position, velocity, acceleration and part of the mass of each surrounding zones. Associated with each zone is the fixed zone mass, relative volume, density, pressure, artificial viscosity, stress deviators, yield stress, internal energy density, distortional energy density, sound speed, and temperature.

Two basic conservation equations are solved - one for each of the two types of calculations. The Lagrange equation of motion, derived from balance of momentum and conservation of mass, is used to update grid point variables. The Lagrange thermal energy equation derived from balance of energy and continuity is used to update zone variables.

Once the geometry, material properties, initial conditions, and boundary conditions are specified, the calculation of the problem is ready to proceed. The first time step that the problem takes has to be prescribed but from that on sub-

sequent time steps are calculated by the code. Physically, the restriction imposed on the length of the time step is that no signal may cross the zone in one time step so that zone reacts only to activity being transmitted from a neighbouring zone. The analysis model is upper part of the half sphere that forms the roof of the containment building. The impact is assumed to be perpendicular to the shell surface at the apex of the shell and the area included to the model extends up to the point where the angle between the radius of the shell and vertical axis is 45^{o}. The outer radius of the shell is 24 m and the thickness of the shell is varied by varying the inner radius. Reinforcement in the shell has been presented by uniform steel layers resisting only membrane forces. The distance of the layers from the shell surfaces is 10 cm. The amount of reinforcement used was 200 kg/m^3.

The finite difference mesh has been designed in order to obtain a sufficient description about the changes of displacement and strain fields. The changes due to impact load are significant only a few meters from load area. So the mesh is finer in the vicinity of the vertical symmetry axis and becomes coarser when the distance from the axis increases. Mesh points are defined according to column and row numbers. The curved lines are columns and straight lines are rows. Boundary conditions are as follows: at the clamped edge both components of velocity are zero and on the symmetry axis the horizontal velocity component is zero. The load area of the impact force is taken to be a circle with an area of 8 m^2. The analysis model is shown in Figure 5.

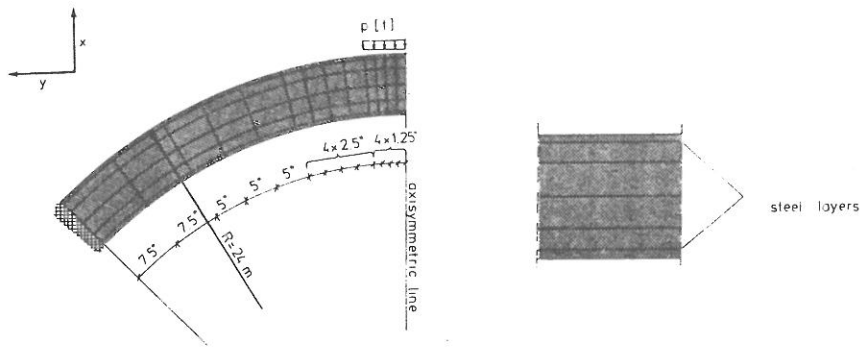

Figure 5. General description of the analysis model.

RESULTS

The method for modelling the reinforcement means that the plastic capacity of the structure is overestimated and the loosening of concrete chunks from the opposite face of the shell wall is effectively prohibited. Because of the circumstances the point of failure has to be concluded by monitoring the values of strains in the concrete. The value of strain signifying the concrete failure was taken to be 0.35 %. If that value is exceeded in a large area failure will take place. Since the capacity of the steel layers to absorb energy is directly proportional to the steel volume and steel strain, it is obvious that for a given amount of reinforcement and assumed strain levels of concrete, the effect of steel is negligible when absorption of energy is considered. This was also verified by direct analysis investigating the dome with constant wall thickness of 1.5 m and using two different values for reinforcement, namely 80 kg/m^3 and 200 kg/m^3. The strain histories of these analyses are presented in Tables 1 and 2. The dome was analysed with three different wall thicknesses: 1.5 m, 1.8 m, and 2.1 m. The amount of reinforcement for all these three analyses was 200 kg/m^3.

Table 1. Development of meridional strain [o/oo] in steel layers for the 1.5 m shell with 80 kg/m^3 reinforcement.

	row / time ms	row 2		row 3		row 4		row 5		row 6	
		upper layer	lower layer	upper layer	lower layer	upper layer	lower layer	upper layer	lower layer	upper layer	lower layer
	19.5	-1.1	0.1	-2.5	-0.3	-1.6	-0.5	-2.2	-0.5	-0.4	-0.8
	24.2	-1.5	-0.2	-3.1	-0.7	-1.2	-0.9	-2.8	-0.9	-0.5	-1.1
	29.1	-1.6	-0.3	-3.5	-0.7	-0.5	-0.9	-2.3	-0.9	-0.6	-1.2
	34	-1.2	0.2	-2.2	-0.1	1.0	-0.2	-1.2	-0.3	-1.0	-0.9
	38.8	-0.2	1.7	0.5	1.7	5.8	1.5	1.6	1.3	1.7	0.1
failure point	48.3	5,2	23.5	12.7	17.8	43.8	5.7	15.2	1.2	10.3	0.8
	52.9	14.2	43.6	33.7	32.5	83	11.6	20.6	1.9	18.0	1.1
	57.5	33.8	71.0	69.3	51.8	135	20.1	22.4	14.0	27.1	1.1
	62.0	60.8	104	113	73.6	193	30.6	22.1	7.2	36.1	1.1
	66.4	91.1	139	155	94.6	248	40.0	21.6	10.0	43.7	0.8
	70.8	123	173	193	113	292	48.5	21.3	13.2	50.0	0.7
	75.2	147	201	201	124	316	54.3	21.4	16.0	54.7	0.8
	78.4	155	215	201	129	315	57.1	20.9	17.8	56.5	0.7

Table 2. Development of meridional strain [o/oo] in steel layers for the 1.5 m shell with 200 km/m^3 reinforcement.

	row / time ms	row 2		row 3		row 4		row 5		row 6	
		upper layer	lower layer	upper layer	lower layer	upper layer	lower layer	upper layer	lower layer	upper layer	lower layer
	20	-1.0	-0.3	1.2	-0.5	-1.1	-0.6	-1.2	-0.6	-0.7	-0.6
	25	-1.1	-0.4	-1.2	-0.7	-1.0	-0.8	-1.1	-0.8	-0.7	-0.9
	30	-0.8	-0.2	-0.7	-0.4	-0.4	-0.4	-0.5	-0.5	-0.6	-0.7
	35	0.3	0.6	0.8	0.6	1.3	0.6	0.7	0.4	0.2	-0.2
	40	1.7	1.7	4.6	1.6	2.6	1.5	2.8	1.4	1.3	0.5
failure point	45	7.0	5.4	11.0	4.4	2.3	1.3	6.1	1.8	3.1	0.8
	50	14.7	11.0	18.2	8.3	4.6	3.1	10.5	1.7	6.2	1.0
	55	29.1	19.0	30.3	13.1	14.3	5.7	10.8	1.4	8.6	1.5
	60	46.7	28.5	43.2	18.4	23.2	8.8	10.7	2.2	11.0	1.7
	65	57.8	35.3	50.4	22.5	26.6	11.3	10.5	4.3	13.1	1.6
	70	59.0	36.5	50.3	23.2	26.0	12.3	9.3	5.8	13.1	1.7
	75	58.2	36.3	50.0	23.1	25.2	12.3	8.7	5.8	12.1	1.5
	80	58.2	35.8	50.1	22.7	25.8	11.9	8.9	5.5	12.4	1.3

In Figures 6 - 8 the deformed state of the structure and stress crosses have been shown at the time point of 80 ms from the beginning of the impact. From the relative lengths of the arms of the stress crosses one can obtain a qualitative picture about the distribution and directions of the principal stresses inside the shell wall.

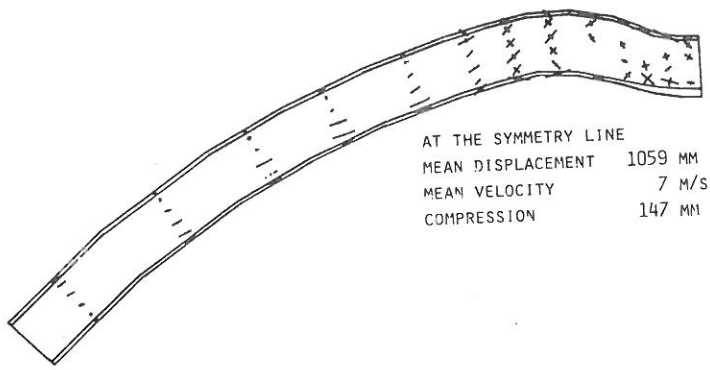

Figure 6. The deformed state of the 1.5 m shell at time 80 ms.

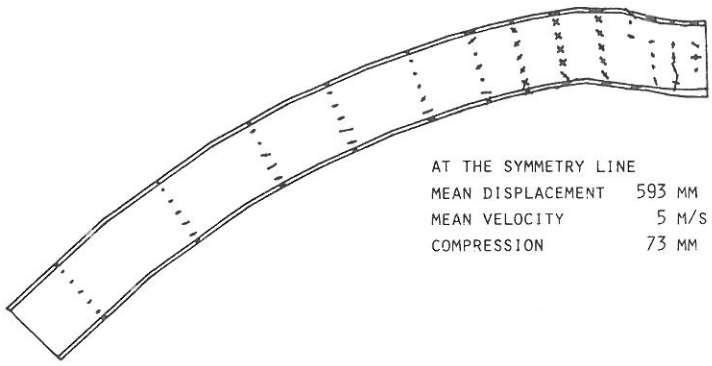

Figure 7. The deformed state of the 1.8 m shell at time 80 ms.

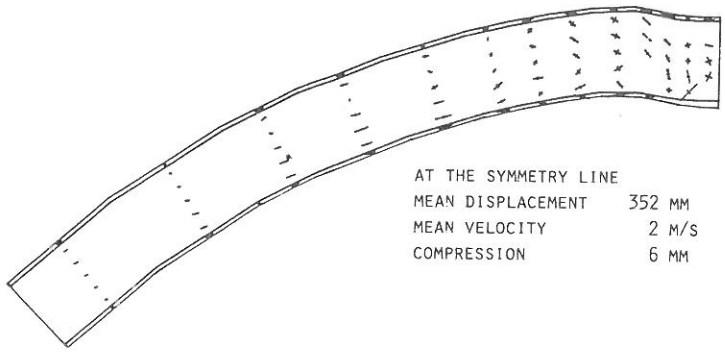

Figure 8. The deformed state of the 2.1 m shell at time 80 ms.

The values of the strains of the steel layers at different time points have been presented in Tables 3 - 4 for the wall thicknesses of 1.8 m and 2.1 m.

After the failure point, presented in the Tables by a double line, the structure resists loads unrealistically because of the modelling of reinforcement by steel layers instead of individual bars. When the wall thickness is 2.1 m the values of strains remain within the allowable range during the whole impact time, excluding a few local exceedings. Moreover, the fact that the strain values are decreasing at the end of the impact (t = 80 ms) supports the conclusion that the containment building is able to withstand the aircraft impact with this wall thickness.

The maximum displacement is about 0.35 m and the compression of the shell wall is about 2 cm at the symmetry axis. First cracks occurred at the time point 50 ms

Table 3. Development of meridional strain [o/oo] in steel layers for the 1.8 m shell with 200 kg/m^3 reinforcement.

time ms \ row	row 2		row 3		row 4		row 5		row 6	
	upper layer	lower layer	upper layer	lower layer	upper layer	lower layer	upper layer	lower layer	upper layer	lower layer
20	-0.4	0.1	-0.5	-0.0	-0.5	-0.0	-0.6	-0.1	-0.2	-0.2
25	-0.5	0.0	-0.5	-0.1	-0.5	-0.2	-0.6	-0.2	-0.2	-0.2
30	-0.6	-0.0	-0.6	-0.1	-0.5	-0.2	-0.6	-0.2	-0.3	-0.3
35	-0.8	-0.2	-0.8	-0.3	-0.7	-0.4	-0.8	-0.4	-0.4	-0.4
40	-1.2	-0.5	-1.0	-0.6	-0.8	-0.7	-1.0	-0.7	-0.7	-0.7
45	-1.0	-0.6	-0.8	-0.7	-0.5	-0.7	-0.8	-0.8	-0.7	-0.9
50	0.6	0.3	1.1	0.3	1.68	-0.4	1.1	0.2	0.4	-0.4
55	3.9	2.1	8.6	2.1	2.5	1.5	4.7	1.8	2.1	0.6
60	10.2	5.8	15.2	4.2	2.2	1.3	9.2	2.0	4.4	1.1
65	14.1	6.3	17.3	4.8	2.9	1.6	-7.5	2.1	5.9	1.2
70	13.9	6.1	17.1	4.7	2.5	1.5	12.4	1.9	6.2	1.3
75	12.7	6.0	15.6	4.5	0.8	1.5	10.7	1.7	5.3	1.3
80	12.6	6.0	15.7	4.5	0.8	1.5	10.7	1.7	5.4	1.4

failure point

Table 4. Development of meridional strain [o/oo] in steel layers for the 2.1 m shell with 200 kg/m^3 reinforcement.

time ms \ row	row 2		row 3		row 4		row 5		row 6	
	upper layer	lower layer	upper layer	lower layer	upper layer	lower layer	upper layer	lower layer	upper layer	lower layer
20	-0.2	0.1	-0.2	0.1	-0.1	0.1	-0.1	-0.0	-0.0	-0.0
25	-0.2	0.2	-0.2	0.1	-0.1	0.1	-0.1	0.0	-0.0	-0.0
30	-0.3	0.2	-0.3	0.1	-0.1	0.1	-0.1	0.0	0.0	-0.1
35	-0.4	0.2	-0.4	0.1	-0.3	-0.0	-0.3	-0.1	-0.1	-0.1
40	-0.8	-0.0	-0.7	-0.0	-0.5	-0.3	-0.7	-0.3	-0.4	-0.3
45	-1.2	-0.4	-1.0	-0.5	-0.8	-0.6	-1.1	-0.6	-0.7	-0.6
50	-1.2	-0.8	-0.9	-0.9	-0.7	-1.0	-1.0	-1.0	-0.8	-1.0
55	-0.3	-0.6	-0.0	-0.7	0.4	-0.6	0.1	-0.7	-0.2	-0.9
60	1.4	0.6	2.6	0.6	2.1	0.7	2.1	0.6	1.0	-0.1
65	4.0	1.4	6.9	1.4	2.0	1.5	3.9	1.6	1.8	0.6
70	4.5	1.5	7.5	1.4	1.9	1.4	4.6	1.8	2.1	0.7
75	3.8	1.2	6.5	1.2	0.7	1.2	3.7	1.4	1.4	0.4
80	3.1	1.1	6.0	1.1	0.1	1.1	3.0	1.4	1.1	0.4

from the beginning of the impact and at the time point 80 ms from the beginning of the impact the concrete has failed both at the bottom and top layers in the vicinity of the impacted area. It is probable that the direction of cracking is radial in inner layers and if that is the case the cracked concrete is prevented to fall apart by the reinforcement layers. The complete prevention of scabbing, meaning the concrete layer outside the bottom steel layer, can be achieved by using an internal steel liner. The obtained sufficient wall thickness of 2.1 m agrees well with the results presented by Alderson et al. /7/ but is slightly more than the value 1.8 m obtained by Hoek and Ree /1/.

In Figure 9 the time histories of total energy, distortional energy and kinetic energy are presented for the analysis of the shell wall with the thickness of 2.1 m.

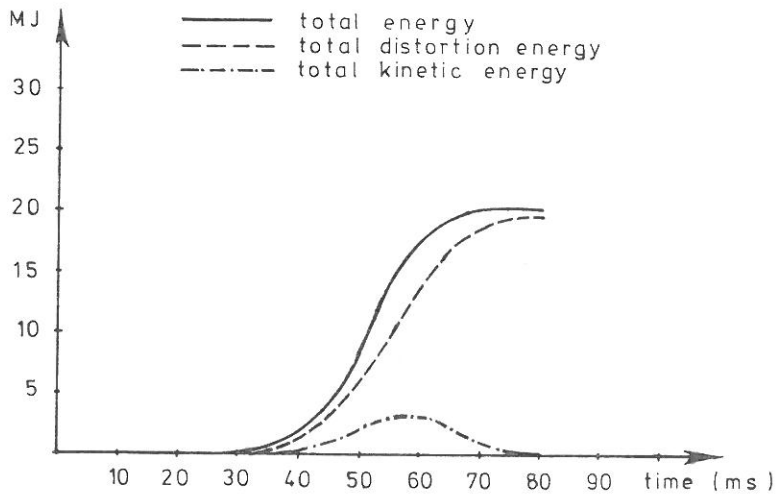

Figure 9. Energy time history of the 2.1 m shell.

In Figure 10 the time histories of mean velocities at the symmetry axis are depicted for wall thicknesses 1.5 m, 1.8 m, and 2.1 m and for the amount of reinforcement of 200 kg/m^3 for each wall thickness.

CONCLUSIONS

The required wall thickness against an aircraft impact is about 2.1 m according to the PISCES analyses carried out in this study. The damages occuring to the shell wall due to the impact, when this thickness is used, are easily repaired. The scabbing of the outermost concrete layer, opposite to the impact face, can be

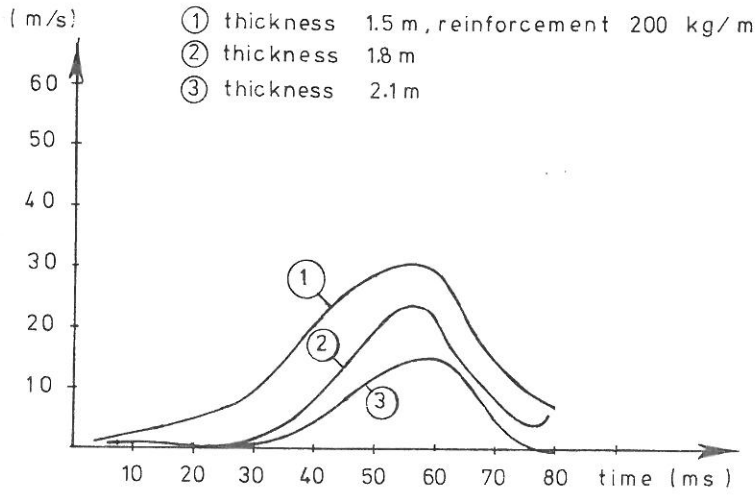

Figure 10. Mean velocity time histories of the apex of the shell.

prevented using a steel liner. The impact will cause highly localized deformations and outside the radius of 3 m deformations are small for all analysed shell thicknesses. The energy absorbed by the structure is mainly distortion energy as can be concluded from Figure 9 and the contribution of the kinetic energy to the total absorbed energy is almost negligible. The energy absorbed by concrete is totally dominant when compared to the energy absorbed by the steel layers. The ratio of these energies is of the order of fifteen. Consequently, the main function of the reinforcement is to ensure the integrity of the structure. Finally, it should be remembered that results obtained are essentially conservative because of the neglection of interaction effects and deformation and inertia effects of the target in the derivation of the load-time function.

REFERENCES

[1] Ree, H. v.d., Hoek, M.J. v.d., Analysis of the behavior of a concrete structure due to an airplane impact and the effects of the reinforcement, 5th SMIRT Conference, Report J 9/5, Berlin 1979.

[2] Structural analysis and design of nuclear plant facilities, J.D. Stevenson, ed., ASCE, 1976.

[3] Drittler, K., Grüner, P., Krivy, J., Berechnung des Stosses eines deformierbaren Flugkörper Modells gegen ein deformierbarens Hindernis, IRS-W-20, April, 1976.

[4] RSK-Leitlinien für Druckwasserreaktoren, 1. Ausgabe, Institut für Reaktorsicherheit det TÜVE.V., April, 1974.

[5] Hoek, M.J. v.d., Modelling of concrete by Mohr-Coulomb Model, Physics International, TN-7802, March, 1978.

[6] PISCES 2DL, Manual A, General description and finite-difference equations, Physics International.

[7] Alderson et al., Reinforced concrete behavior due to missile impact, 4th SMIRT Conference, Report J 7/7, San Francisco, 1977.

Jari Puttonen, tekn.lis., Imatran Voima Oy
Pentti Varpasuo, tekn.tri, Imatran Voima Oy